EUROPEAN ORGANIZATION FOR NUCLEAR RESEARCH

CERN-EP/90-54
24 April 1990

Heavy Flavour Production in Z Decays

The ALEPH Collaboration*

Abstract

From an analysis of inclusive leptons in data collected by the ALEPH detector at LEP, we measure the fractions of $b\bar{b}$ and $c\bar{c}$ events in hadronic Z decays. The $b\bar{b}$ fraction times semileptonic branching ratio is measured to be $\mathrm{Br}(b \to e) \cdot \Gamma_{b\bar{b}}/\Gamma_{\mathrm{had}} = 0.0224 \pm 0.0016 \pm 0.0010$. Assuming a b semileptonic branching ratio of 0.102 ± 0.010 gives $\Gamma_{b\bar{b}}/\Gamma_{\mathrm{had}} = 0.220 \pm 0.016 \pm 0.024$, in good agreement with the Standard-Model prediction of 0.217. The $c\bar{c}$ fraction times semileptonic branching ratio is measured to be $\mathrm{Br}(c \to e) \cdot \Gamma_{c\bar{c}}/\Gamma_{\mathrm{had}} = 0.0133 \pm 0.0040^{+0.0038}_{-0.0031}$. Assuming a c semileptonic branching ratio of 0.090 ± 0.013 gives $\Gamma_{c\bar{c}}/\Gamma_{\mathrm{had}} = 0.148 \pm 0.044^{+0.045}_{-0.038}$, in agreement with the Standard-Model prediction of 0.171.

(Submitted to Physics Letters B)

*See the following pages for the list of authors.

The ALEPH Collaboration

D. Decamp, B. Deschizeaux, C. Goy, J.-P. Lees, M.-N. Minard

Laboratoire de Physique des Particules (LAPP), IN²P³-CNRS, 74019 Annecy-le-Vieux Cedex, France

J.M. Crespo, M. Delfino, E. Fernandez, P. Mato, R. Miquel, Ll.M. Mir, S. Orteu, A. Pacheco, J.A. Perlas, E. Tubau

Laboratorio de Fisica de Altas Energias, Universidad Autonoma de Barcelona, 08193 Bellaterra (Barcelona), Spain[9]

M.G. Catanesi, M. de Palma, A. Farilla, G. Iaselli, G. Maggi, S. Natali, S. Nuzzo, A. Ranieri, G. Raso, F. Romano, F. Ruggieri, G. Selvaggi, L. Silvestris, P. Tempesta, G. Zito

INFN Sezione di Bari e Dipartimento di Fisica dell' Università, 70126 Bari, Italy

Y. Gao, H. Hu, D. Huang, S. Jin, J. Lin, T. Ruan, T. Wang, W. Wu, Y. Xie, D. Xu, R. Xu, J. Zhang, Z. Zhang, W. Zhao

Institute of High-Energy Physics, Academia Sinica, Beijing, The People's Republic of China[10]

H. Albrecht[2], W.B. Atwood[3], F. Bird, E. Blucher, D. Brown, T.H. Burnett[4], H. Drevermann, R.W. Forty, Ll. Garrido, C. Grab, R. Hagelberg, S. Haywood, B. Jost, M. Kasemann, G. Kellner, J. Knobloch, A. Lacourt, I. Lehraus, T. Lohse, D. Lüke[2], A. Marchioro, M. Martinez, J. May[2], S. Menary, A. Minten, A. Miotto, P. Palazzi, M. Pepe-Altarelli, F. Ranjard, A. Roth, J. Rothberg[4], H. Rotscheidt, W. von Rüden, R. St.Denis, D. Schlatter, M. Takashima, M. Talby[5], H. Taureg, W. Tejessy, H. Wachsmuth, S. Wasserbaech, S. Wheeler, W. Wiedenmann, W. Witzeling, J. Wotschack

European Laboratory for Particle Physics (CERN), 1211 Geneva 23, Switzerland

Z. Ajaltouni, M. Bardadin-Otwinowska, A. Falvard, P. Gay, P. Henrard, J. Jousset, B. Michel, J-C. Montret, D. Pallin, P. Perret, J. Proriol, F. Prulhière

Laboratoire de Physique Corpusculaire, Université Blaise Pascal, IN²P³-CNRS, Clermont-Ferrand, 63177 Aubière, France

J.D. Hansen, J.R. Hansen, P.H. Hansen, R. Møllerud, B.S. Nilsson, G. Petersen

Niels Bohr Institute, 2100 Copenhagen, Denmark[11]

I. Efthymiopoulos, E. Simopoulou, A. Vayaki

Nuclear Research Center Demokritos (NRCD), Athens, Greece

J. Badier, A. Blondel, G. Bonneaud, J. Bourotte, F. Braems, J.C. Brient, M.A. Ciocci, G. Fouque, R. Guirlet, A. Rougé, M. Rumpf, R. Tanaka, H. Videau, I. Videau[1]

Laboratoire de Physique Nucléaire et des Hautes Energies, Ecole Polytechnique, IN²P³-CNRS, 91128 Palaiseau Cedex, France

D.J. Candlin

Department of Physics, University of Edinburgh, Edinburgh EH9 3JZ, United Kingdom[12]

G. Parrini

Dipartimento di Fisica, Università di Firenze, INFN Sezione di Firenze, 50125 Firenze, Italy

M. Corden, C. Georgiopoulos, J.H. Goldman, M. Ikeda, J. Lannutti, D. Levinthal[17], M. Mermikides, L. Sawyer, G. Stimpfl

Supercomputer Computations Research Institute and Dept. of Physics, Florida State University, Tallahassee, FL 32306, USA[14,15,16]

A. Antonelli, R. Baldini, G. Bencivenni, G. Bologna[6], F. Bossi, P. Campana, G. Capon, V. Chiarella, G. De Ninno, B. D'Ettorre-Piazzoli[7], G. Felici, P. Laurelli, G. Mannocchi[7], F. Murtas, G.P. Murtas, G. Nicoletti, L. Passalacqua, P. Picchi[6], P. Zografou

Laboratori Nazionali dell'INFN (LNF-INFN), 00044 Frascati, Italy

B. Altoon, O. Boyle, A.W. Halley, I. ten Have, J.L. Hearns, I.S. Hughes, J.G. Lynch, W.T. Morton, C. Raine, J.M. Scarr, K. Smith[1], A.S. Thompson

Department of Physics and Astronomy, University of Glasgow, Glasgow G12 8QQ, United Kingdom[12]

B. Brandl, O. Braun, R. Geiges, C. Geweniger, P. Hanke, V. Hepp, E.E. Kluge, Y. Maumary, M. Panter, A. Putzer, B. Rensch, A. Stahl, K. Tittel, M. Wunsch

Institut für Hochenergiephysik, Universität Heidelberg, 6900 Heidelberg, Fed. Rep. of Germany[18]

A.T. Belk, R. Beuselinck, D.M. Binnie, W. Cameron[1], M. Cattaneo, P.J. Dornan, S. Dugeay, A.M. Greene, J.F. Hassard, S.J. Patton, J.K. Sedgbeer, G. Taylor, I.R. Tomalin, A.G. Wright

Department of Physics, Imperial College, London SW7 2BZ, United Kingdom[12]

P. Girtler, D. Kuhn, G. Rudolph

Institut für Experimentalphysik, Universität Innsbruck, 6020 Innsbruck, Austria[20]

C.K. Bowdery[1], T.J. Brodbeck, A.J. Finch, F. Foster, G. Hughes, N.R. Keemer, M. Nuttall, B.S. Rowlingson, T. Sloan, S.W. Snow

Department of Physics, University of Lancaster, Lancaster LA1 4YB, United Kingdom[12]

T. Barczewski, L.A.T. Bauerdick, K. Kleinknecht, B. Renk, S. Roehn, H.-G. Sander, M. Schmelling, F. Steeg

Institut für Physik, Universität Mainz, 6500 Mainz, Fed. Rep. of Germany[18]

J-P. Albanese, J-J. Aubert, C. Benchouk, A. Bonissent, D. Courvoisier, F. Etienne, E. Matsinos, S. Papalexiou, P. Payre, B. Pietrzyk, Z. Qian

Centre de Physique des Particules, Faculté des Sciences de Luminy, IN²P³-CNRS, 13288 Marseille, France

W. Blum, P. Cattaneo, G. Cowan, B. Dehning, H. Dietl, M. Fernandez-Bosman, A. Jahn, E. Lange, G. Lütjens, G. Lutz, W. Männer, H-G. Moser, Y. Pan, R. Richter, A.S. Schwarz, R. Settles, U. Stiegler, U. Stierlin, J. Thomas

Max-Planck-Institut für Physik und Astrophysik, Werner-Heisenberg-Institut für Physik, 8000 München, Fed. Rep. of Germany[18]

V. Bertin, G. de Bouard, J. Boucrot, O. Callot[1], X. Chen, A. Cordier, M. Davier, G. Ganis, J.-F. Grivaz, Ph. Heusse, P. Janot, V. Journé, D.W. Kim[21], J. Lefrançois, A.-M. Lutz, J.-J. Veillet, F. Zomer

Laboratoire de l'Accéléateur Linéaire, Université de Paris-Sud, IN²P³-CNRS, 91405 Orsay Cedex, France

S.R. Amendolia, G. Bagliesi, G. Batignani, L. Bosisio, U. Bottigli, C. Bradaschia, I. Ferrante, F. Fidecaro, L. Foà[1], E. Focardi, F. Forti, A. Giassi, M.A. Giorgi, F. Ligabue, A. Lusiani, E.B. Mannelli, P.S. Marrocchesi, A. Messineo, F. Palla, G. Sanguinetti, J. Steinberger, R. Tenchini, G. Tonelli, G. Triggiani

Dipartimento di Fisica dell'Università, INFN Sezione di Pisa, e Scuola Normale Superiore, 56010 Pisa, Italy

J.M. Carter, M.G. Green, P.V. March, T. Medcalf, M.R. Saich, J.A. Strong[1], R.M. Thomas, T. Wildish

Department of Physics, Royal Holloway & Bedford New College, University of London, Surrey TW20 OEX, United Kingdom[12]

D.R. Botterill, R.W. Clifft, T.R. Edgecock, M. Edwards, S.M. Fisher, J. Harvey, T.J. Jones, P.R. Norton, D.P. Salmon, J.C. Thompson

Particle Physics Dept., Rutherford Appleton Laboratory, Chilton, Didcot, OXON OX11 OQX, United Kingdom[12]

B. Bloch-Devaux, P. Colas, C. Klopfenstein, E. Lançon, E. Locci, S. Loucatos, L. Mirabito, E. Monnier, P. Perez, F. Perrier, J. Rander, J.-F. Renardy, A. Roussarie, J.-P. Schuller

Département de Physique des Particules Élémentaires, CEN-Saclay, 91191 Gif-sur-Yvette Cedex, France[19]

J.G. Ashman, C.N. Booth, F. Combley, M. Dinsdale, J. Martin, D. Parker, L.F. Thompson

Department of Physics, University of Sheffield, Sheffield S3 7RH, United Kingdom[12]

S. Brandt, H. Burkhardt[1], C. Grupen[1], E. Neugebauer, U. Schäfer, H. Seywerd

Fachbereich Physik, Universität Siegen, 5900 Siegen, Fed. Rep. of Germany[18]

B. Gobbo, F. Liello, E. Milotti, L. Rolandi[1]

Dipartimento di Fisica, Università di Trieste e INFN Sezione di Trieste, 34127 Trieste, Italy

L. Bellantoni, J.F. Boudreau, D. Cinabro, J.S. Conway, D.F. Cowen, Z. Feng, J.L. Harton, J. Hilgart, R.C. Jared[8], R.P. Johnson, B.W. LeClaire, Y.B. Pan, T. Parker, J.R. Pater, Y. Saadi, V. Sharma, J.A. Wear, F.V. Weber, Sau Lan Wu, S.T. Xue, G. Zobernig

Department of Physics, University of Wisconsin, Madison, WI 53706, USA[13]

[1] Now at CERN.
[2] Permanent address: DESY, Hamburg, Fed. Rep. of Germany.
[3] On leave of absence from SLAC, Stanford, CA 94309, USA.
[4] On leave of absence from University of Washington, Seattle, WA 98195, USA.
[5] Also Centre de Physique des Particules, Faculté des Sciences, Marseille, France
[6] Also Istituto di Fisica Generale, Università di Torino, Torino, Italy.
[7] Also Istituto di Cosmo-Geofisica del C.N.R., Torino, Italy.
[8] Now at INFN Milano.
[8] Permanent address: LBL, Berkeley, CA 94720, USA.
[9] Supported by CAICYT, Spain.
[10] Supported by the National Science Foundation of China.
[11] Supported by the Danish Natural Science Research Council.
[12] Supported by the UK Science and Engineering Research Council.
[13] Supported by the US Department of Energy, contract DE-AC02-76ER00881.
[14] Supported by the US Department of Energy, contract DE-FG05-87ER40319.
[15] Supported by the NSF, contract PHY-8451274.
[16] Supported by the US Department of Energy, contract DE-FC0S-85ER250000.
[17] Supported by SLOAN fellowship, contract BR 2703.
[18] Supported by the Bundesministerium für Forschung und Technologie, Fed. Rep. of Germany.
[19] Supported by the Institut de Recherche Fondamentale du C.E.A..
[20] Supported by Fonds zur Förderung der wissenschaftlichen Forschung, Austria.
[21] Supported by Non Directed Research Fund, Korea Res. Fund, 1989.

1 Introduction

With the recent commissioning of the LEP e^+e^- collider, the Z total hadronic decay width has been precisely measured [1,2]. The results are consistent with the Standard-Model [3] expectations for Z decay to five flavours of quark-antiquark pairs ($u\bar{u}$, $d\bar{d}$, $s\bar{s}$, $c\bar{c}$ and $b\bar{b}$). It is important to measure, in addition, the Z coupling to the individual quark flavours [4,5], which in the Standard Model depends on the weak isospin of the quark. This letter reports a measurement of the fractions of $b\bar{b}$ and $c\bar{c}$ events in hadronic Z decays ($\Gamma_{b\bar{b}}/\Gamma_{\rm had}$ and $\Gamma_{c\bar{c}}/\Gamma_{\rm had}$) using the ALEPH detector at LEP.

The measurement is based on a study of inclusive electrons and muons in a sample of about 25000 hadronic events, corresponding to an integrated luminosity of $1.17\,{\rm pb}^{-1}$, collected at center-of-mass energies between 88.3 and 94.3 GeV. Semileptonic decays of heavy quarks are characterized by leptons of high average momentum p and transverse momentum $p_\perp$, reflecting the hard fragmentation of the c and b quarks and the large masses of the c and b hadrons. By fitting the p, $p_\perp$ spectrum of leptons observed in hadronic decays of the Z, the c and b contributions can be disentangled from each other and from the light-quark (u, d, s) background, yielding measurements of the $b\bar{b}$ and $c\bar{c}$ fractions, and also of b and c fragmentation parameters.

2 The ALEPH Detector

The ALEPH detector is described in detail in Ref. 6. Only a brief description of those features relevant to this analysis is given here.

Closest to the beam collision region is the inner tracking chamber (ITC), with eight concentric drift chamber layers. Surrounding this is a large time projection chamber (TPC), a cylindrical drift chamber with 18 multi-wire proportional chambers (sectors) at each end. The sector cathode planes are segmented into 21 concentric rows of pads, which provide measurements of up to 21 space points for charged particles traversing the full radius ($|\cos\theta| < 0.79$). Measurements from dimuon production, $e^+e^- \to \mu^+\mu^-$, for tracks crossing both the ITC and the TPC yield a momentum resolution of $\delta p/p^2 = 0.0011\ ({\rm GeV/c})^{-1}$. Charged particles are measured with a high efficiency over 96% of the solid angle, since those within $|\cos\theta| < 0.96$ cross all 8 layers of the ITC and at least 4 pad rows in the TPC. Up to 330 measurements of the specific ionization (dE/dx) for each charged particle are provided by the TPC sense wires. In hadronic events, the dE/dx resolution obtained is 5.2% for 330 ionization samples.

The Electromagnetic Calorimeter (ECAL) is a highly segmented sandwich

of planar proportional chambers and lead plates. It has a thickness of 22 radiation lengths and covers the angular region $|\cos\theta| < 0.98$. The energy and position of electromagnetic showers are measured using 3×3 cm^2 cathode pads connected internally to form projective towers. Each tower is read out in three stacks corresponding to 4, 9 and 9 radiation lengths. For electromagnetic showers, the energy resolution is measured to be $\delta E/E = 0.18/\sqrt{E}$, and the angular resolution is typically $4\,\mathrm{mrad}/\sqrt{E}$ (E in GeV). The ITC, TPC and ECAL are enclosed in a superconducting solenoid providing an axial magnetic field of 1.5 Tesla.

Outside the coil the 120 cm thick return yoke is instrumented with 23 layers of 1×1 cm^2 streamer tubes to form the hadron calorimeter, HCAL. It covers almost the full solid angle, although only the barrel section where the digital readout was fully operational for the 1989 runs is used for the present analysis. This covers the angular region $|\cos\theta| < 0.61$. The digital readout from the streamer tubes, with a 1 cm pitch, is used to identify muon candidates by tracking them in the plane transverse to the beam.

The triggers for hadronic Z decays are described in detail elsewhere [1]. They depend upon the energy deposited in the ECAL, a correlation between a track in the ITC and energy in the corresponding azimuthal sector of ECAL, or a correlation between a track in the ITC and a penetration signal from a corresponding sector in the HCAL. The overall trigger efficiency for hadronic Z decays is effectively 100%.

3 Event Selection

Hadronic events are selected using charged tracks reconstructed in the TPC as described in Ref. 1, except that the cut on the visible charged energy is increased from 10% to 20% of the total center-of-mass energy. This results in an overall efficiency of 94.8%, which according to Monte Carlo is independent of quark flavour to better than 1%. The background from $\tau\bar{\tau}$ and two-photon events is estimated by Monte Carlo to be less than 0.3%.

The Monte Carlo generator used in this analysis has been developed within ALEPH specifically for event simulation in heavy flavour studies. It is based on DYMU [7] to simulate initial and final state radiation in the reaction $e^+e^- \rightarrow Z \rightarrow q\bar{q}$ and on the Lund JETSET 6.3 (parton shower) [8] model to generate the parton cascade and hadron production. The fragmentation of b and c quarks is described by the parameterization of Peterson *et al.* [9],

$$f(z) \propto \frac{1}{z[1-1/z-\epsilon_q/(1-z)]^2} \quad \text{with} \quad z = \frac{(E+p_{\parallel})_{\mathrm{hadron}}}{(E+p)_{\mathrm{quark}}}, \qquad (1)$$

where $(E+p)_{\text{quark}}$ is the quark energy and momentum after the parton cascade, $(E+p_{\parallel})_{\text{hadron}}$ is the hadron energy and momentum component parallel to the quark direction, and ϵ_q is a parameter to be determined experimentally for each heavy quark. The JETSET 6.3 program has been modified to include an improved formulation of B semileptonic decays and updated decay branching ratios for charm and bottom mesons. The fragmentation parameters and the leptonic decay branching ratios employed were based on data available from experiments at lower energies [10].

The Monte Carlo includes a detailed simulation of the ALEPH detector. In particular, the calorimeter responses have been tuned using both test-beam and LEP data. Whenever possible, however, estimates of lepton selection efficiency and backgrounds in this analysis are obtained using data.

In order to tag leptons from c and b decays, use is made of the fact that the semileptonic decay of a heavy-flavour hadron frequently results in a lepton with a high transverse momentum with respect to the hadron direction. Jets are defined using charged tracks and the scaled-invariant-mass clustering algorithm [11]. Monte Carlo studies have shown that this procedure accurately reconstructs the axis of the lepton's ancestor. The transverse momentum of the lepton, $p_{\perp}$, is determined by removing the lepton from its jet, re-evaluating the jet momentum and then calculating the $p_{\perp}$ of the lepton with respect to this axis (resulting in a $p_{\perp}$ scale which is different from that of, for example, Ref. [5]). When this procedure is applied to charged tracks, Monte Carlo simulations predict that the separation between the leptons from b quarks and the background is improved with respect to a method in which $p_{\perp}$ is calculated without removing the lepton from the definition of the jet axis.

4 Electron Identification

Electron identification is performed in ALEPH using two independent measurements: the energy deposition in the ECAL and the energy loss ($\mathrm{d}E/\mathrm{d}x$) in the TPC. The two methods are complementary, the former being most effective at high momentum (above 5 GeV/c) and the latter at low momentum.

The high granularity of the ECAL, in which each projective tower covers approximately $1^\circ \times 1^\circ$ and is read out in three longitudinal stacks, provides good e–π separation in jets. Two variables are defined to measure the degree to which the energy deposition in the neighbourhood of an extrapolated track conforms with that expected for an electron. The first, R_T, compares the measured momentum to the energy deposited in the four towers closest to the extrapolated track, and the second, R_L, provides a measure of the degree to which the longitudinal shower profile matches that expected for an electron.

To evaluate these quantities, each charged track is extrapolated to each ECAL stack, and the energy E_i deposited in the four towers closest to the extrapolation is recorded for each of the three stacks i. Test-beam data show that the variable

$$X = \frac{E_0}{p}, \quad \text{with} \quad E_0 = \sum_{i=1}^{3} E_i \,, \tag{2}$$

has a Gaussian distribution for electrons of a given energy. The mean, $\langle X \rangle$, is 0.83 independent of angle and momentum for $p > 2\,\mathrm{GeV/c}$, while a parameterization of the variance, $\sigma^2(X)$, with respect to momentum is obtained from the test-beam measurements. Thus, for electrons, the variable

$$R_T = \frac{X - \langle X \rangle}{\sigma(X)} \tag{3}$$

is normally distributed with zero mean and unit variance. Due to the high granularity of the ECAL, this variable reflects the compactness of an electromagnetic shower as well as giving a measurement of the momentum-energy balance.

The variable R_L is related to the inverse of the mean position A of the longitudinal energy deposition:

$$A = \frac{E_0}{\sum_{i=1}^{3} E_i S_i} \,, \tag{4}$$

where S_i is the mean longitudinal position of the shower in stack i. The test-beam data show that, for electrons of a given energy, A is Gaussian distributed. A parameterization of $\langle A \rangle$ and $\sigma(A)$ is obtained from the test-beam measurements, giving a variable

$$R_L = \frac{A - \langle A \rangle}{\sigma(A)} \tag{5}$$

which, for electrons, is normally distributed with zero mean and unit variance.

To verify the performance of these selection variables in the environment of hadronic jets, their distributions are compared with Monte Carlo simulations. The R_L distribution agrees well. Making the cut $-2.4 < R_L < 3.0$ yields the distribution shown in Fig. 1.a, which shows the behavior of R_T as a function of track momentum. The accumulation of electrons around $R_T = 0$ is well separated from the hadron background above $2\,\mathrm{GeV/c}$. Figure 2.a shows a comparison between the R_T distribution for tracks with $p > 2\,\mathrm{GeV/c}$ and the Monte Carlo simulation, normalized to the number of hadronic events. The disagreement between Monte Carlo and data below the electron peak indicates that the simulation may not give an accurate prediction of the background. In fact, measurements by $\mathrm{d}E/\mathrm{d}x$, described below, show that the background is

overestimated by a factor which ranges between 2.0 at $p = 2.5\,\mathrm{GeV/c}$ and 1.1 at $p = 9.0\,\mathrm{GeV/c}$.

Electron candidates are selected by the cuts

$$R_T > -3.0 \quad \text{and} \quad -2.4 < R_L < 3.0\,. \tag{6}$$

There is no upper cut on R_T in order not to reject isolated electrons which have emitted hard bremsstrahlung photons before entering the tracking chambers or electrons which overlap with other calorimetric energy deposits.

Electron identification using ECAL is supplemented with the $\mathrm{d}E/\mathrm{d}x$ information from the TPC. The measured $\mathrm{d}E/\mathrm{d}x$, I_m, is defined to be the 60% truncated mean of the individual wire measurements. Only tracks associated with at least 80 isolated wire hits are considered in the $\mathrm{d}E/\mathrm{d}x$ analysis.

The dependence of the mean value of I_m on particle velocity is measured from data. The momentum region of interest in this measurement is on the relativistic rise for pions and kaons, while electrons always are distributed about the plateau position $\langle I_\mathrm{e}\rangle$, lying a factor of 1.58 above the minimum. By taking the difference of the measured $\mathrm{d}E/\mathrm{d}x$ with that expected for an electron, a selection variable is defined which is normally distributed for electrons:

$$R_I = \frac{I_\mathrm{m} - \langle I_\mathrm{e}\rangle}{\sigma(I)}\,. \tag{7}$$

Hadronic data are used to obtain a parameterization of $\sigma(I)/I$, which depends only on the number of wire samples. Figure 1.b shows a distribution of R_I versus momentum for all tracks passing the ECAL electron selection. At low momentum there is a significant background of hadrons which have passed the ECAL criteria but can be rejected by the $\mathrm{d}E/\mathrm{d}x$ measurement.

The $\mathrm{d}E/\mathrm{d}x$ serves two purposes in the inclusive electron analysis. First, since the $\mathrm{d}E/\mathrm{d}x$ identification is independent of that of the ECAL, it provides a measurement of the hadron background. Second, by requiring that all electron candidates satisfy $R_I > -2.5$ as well as the ECAL cuts of Eqn. 6, the background of misidentified hadrons can be significantly reduced.

The efficiency of the ECAL electron selection criteria is monitored by using electron pairs from photon conversions in the chamber walls between the ITC and TPC. The measured efficiency is $80 \pm 2\%$, with negligible momentum dependence above $2\,\mathrm{GeV/c}$. This result agrees well with Monte Carlo predictions, which show no significant dependence on p or $p_\perp$.

For identification by $\mathrm{d}E/\mathrm{d}x$, the main source of inefficiency is the requirement of at least 80 isolated wire hits, for which there is a strong dependence on p and $p_\perp$. It is precisely measured from data by counting the fraction of all tracks which give more than 80 wire hits. Tracks from recognized photon

p	$p_\perp$	0-0.5	0.5-1.0	1.0-2.0	2.0-5.0
2-3	ϵ'_e	51.0 ±2.0	64.4 ±2.6	73.2 ±2.9	74.2 ±3.0
	ϵ_π	0.70 ±0.04	0.70 ±0.04	0.57 ±0.12	0.57 ±0.12
	ϵ'_π	0.038±0.002	0.038±0.002	0.019±0.004	0.019±0.004
3-5	ϵ'_e	47.6 ±1.9	59.1 ±2.4	68.8 ±2.8	74.3 ±3.0
	ϵ_π	0.62 ±0.05	0.62 ±0.05	0.32 ±0.07	0.32 ±0.07
	ϵ'_π	0.088±0.007	0.088±0.007	0.039±0.009	0.039±0.009
5-7	ϵ'_e	41.8 ±1.7	52.6 ±2.1	65.4 ±2.6	74.0 ±3.0
	ϵ_π	0.59 ±0.08	0.59 ±0.08	0.60 ±0.13	0.60 ±0.13
	ϵ'_π	0.17 ±0.02	0.17 ±0.02	0.16 ±0.04	0.16 ±0.04
7-11	ϵ'_e	37.1 ±1.5	46.5 ±1.9	57.9 ±2.3	70.6 ±2.8
	ϵ_π	0.60 ±0.11	0.60 ±0.11	0.60 ±0.11	0.60 ±0.11
	ϵ'_π	0.25 ±0.05	0.25 ±0.05	0.25 ±0.05	0.25 ±0.05
11-21	ϵ'_e	38.9 ±1.6	41.8 ±1.7	52.2 ±2.1	63.1 ±2.5
	ϵ_π	0.42 ±0.12	0.42 ±0.12	0.42 ±0.12	0.42 ±0.12
	ϵ'_π	0.24 ±0.07	0.24 ±0.07	0.24 ±0.07	0.24 ±0.07

Table 1: The combined efficiency for electron identification by ECAL plus $\mathrm{d}E/\mathrm{d}x$ plus pair rejection (ϵ'_e), the hadron misidentification probability for the ECAL alone (ϵ_π), and the hadron misidentification probability for the ECAL plus $\mathrm{d}E/\mathrm{d}x$ (ϵ'_π). The efficiency for the ECAL selection alone (ϵ_e) is $80 \pm 2\%$, independent of p and $p_\perp$. All efficiencies are given in percent, and p and $p_\perp$ are in units of GeV/c. Where there are insufficient data, a coarser binning is used for ϵ_π and ϵ'_π than for ϵ'_e, such that identical values are quoted here in several neighbouring bins.

conversions are excluded, because the e^+e^- pairs do not separate in z and therefore have an abnormally low probability of producing isolated wire hits. The results are in good agreement with the Monte Carlo simulation. The additional inefficiency from the cut $R_I > -2.5$ is only 1%, as has been verified from measurements using electrons from Bhabha scattering and photon conversions. The overall electron identification efficiency in bins of p and $p_\perp$ is given in Table 1 and has a 4% relative systematic uncertainty.

Contamination of the prompt electron signal is caused by electrons from photon conversions and π^0 decays plus a residual background from hadrons which pass the electron selection cuts. The background from photon conversions and Dalitz pairs is reduced with three cuts:

- candidates are removed if their distance of closest approach to the interaction point in the x–y projection is larger than 5 mm;
- candidates are removed if more than three ITC drift cells through which the track passed gave no signal;
- candidates are removed if they form an invariant mass of less than 20 MeV/c^2 when paired with any oppositely charged track which is consistent with coming from a common vertex.

For $p > 2\,\mathrm{GeV/c}$, the Monte Carlo predicts that these cuts remove 87% of all electrons from photon conversions and 47% of those from π^0 decays. The distribution of the radius of the vertex of detected photon conversions and the distribution of p, $p_\perp$ for candidates removed by the three cuts agree well, in shape and in quantity, with the prediction of the simulation, even when the cuts are varied over a wide range. The systematic uncertainty in the Monte Carlo prediction of the remaining background from non-prompt electrons is estimated to be $\pm 4\%$ in the low-$p_\perp$ bins, rising to $\pm 50\%$ at very high $p_\perp$, where the background is less than 3% of the signal. On average, only 2.4% of the signal is removed by these cuts.

The hadron misidentification probability is measured as a function of p and $p_\perp$ by a fit to the R_I distribution of electron candidates selected by the ECAL. The shape of the background component is obtained from a histogram of R_I for all tracks which fail the ECAL electron selection. This assumes only that the ratio of kaons to pions is not significantly affected by the ECAL cuts. The electron signal component, after calibrating the resolution and the position of the $\mathrm{d}E/\mathrm{d}x$ plateau, is Gaussian with zero mean and unit width. In the fit, only the amplitudes of the electron signal and the hadron background are allowed to vary. The distributions shown in Fig. 2.b demonstrate the quality of this procedure for all electrons with $3 < p < 7\,\mathrm{GeV/c}$.

The fitted level of the background gives directly the hadron misidentification probability of the ECAL selection, while the fraction of background remaining above $R_I = -2.5$ gives an estimate of the misidentification probability of the selection using both ECAL and $\mathrm{d}E/\mathrm{d}x$. The systematic error in the background prediction is derived by repeating the fits with the position and width of the gaussian contribution allowed to vary freely, in order to take into account uncertainty in the calibration of the $\mathrm{d}E/\mathrm{d}x$ response to the signal. The results of this analysis are presented in Table 1.

5 Muon Identification

When a charged particle crosses a plane of streamer tubes in the hadron calorimeter, typically between one and four adjacent tubes give hits, forming a cluster. Muons are characterized by a track of such clusters penetrating through all 23 layers of iron. The present analysis is restricted to the barrel region (52° to 128° polar angle), where the digital readout of the streamer tubes was fully operational for the 1989 runs.

The algorithm employed extrapolates all charged tracks with momenta above 1 GeV/c through the electromagnetic calorimeter, the coil and the hadron calorimeter, taking into account the reverse magnetic field in the iron yoke of the HCAL. A cone three times larger than the r.m.s. displacement due to multiple scattering is defined along the extrapolated track, and muon candidates are selected according to the distribution of fired planes within the cone. A plane is only considered to have fired if the cluster is composed of no more than four hits. A track is considered to be a muon candidate if

- more than 9 planes fire in total,
- more than 4 of the last 10 planes fire,
- and at least 1 of the last 3 planes fire.

The single plane efficiency varied slightly both over the detector and over the data taking period, so an efficiency map was produced using a clean sample of dimuon events, $e^+e^- \rightarrow \mu^+\mu^-$. This gave an average plane efficiency of approximately 70%, with half of the inefficiency resulting from geometrical effects. When used in the Monte Carlo simulation of the HCAL, the map produces good agreement with the dimuon data for both the distribution of the total number of fired planes and the number which fire in the last 10.

For 12% of muons with $p > 3\,\mathrm{GeV/c}$, the multiple scattering cone overlaps with that of an adjacent hadron, giving the possibility that the wrong TPC track is associated with the HCAL digitizations. To resolve the ambiguity in such cases, a likelihood for the match between the track and the HCAL hits is evaluated for each track, and only the candidate having the largest value is kept. The Monte Carlo simulation predicts that this procedure correctly resolves the ambiguity in 85% of the cases.

The hadron contamination to the muon sample is due to three effects:

1. pion or kaon decay, with the muon faking a prompt muon,
2. sail-through: a hadron crossing the whole calorimeter without interacting,

3. punch-through: an interacting hadron producing one or more secondaries which exit the calorimeter within the multiple scattering cone.

Both the decays and sail-through hadrons result in a muon-like pattern in the calorimeter. However, their number is well predicted by the Monte Carlo, and their contribution to the final sample can be estimated with sufficient accuracy.

The calorimeter's response to the hadron punch-through is more difficult to simulate, although the detector simulation gives reasonable agreement with test-beam data. An additional cut is therefore introduced to reduce the size of this background based on the differing patterns of hits in the HCAL left by muons and interacting hadrons. It employs a search in the last ten layers of the HCAL for evidence of hadronic interactions. Cuts are made on both the number of hits in excess of those expected from a muon and the number of unassociated clusters found in a road ± 25 cm around the measured position of the muon candidate. The road width is determined from the typical transverse size of a hadronic shower. For those muon candidates which pass all cuts excluding the requirements on the number of hits in the last ten planes, the number of planes firing in the last 10 agrees well with the Monte Carlo simulation, as shown in Fig. 3.

After all the cuts, the ability of the Monte Carlo to reproduce the background is checked using a sample of pions with $p > 3$ GeV/c from K^0_s decay and also by a visual scan of the remaining candidates. In the data $(0.9 \pm 0.2)\%$ of the pions from the K^0_s satisfy the muon criteria, compared with $(0.85 \pm 0.10)\%$ in the Monte Carlo. However, due to the relatively low momenta of these pions, this test is primarily sensitive to decay and sail-through background. The scan shows that the residual punch-through background is in reasonable agreement with the 4% level predicted by the Monte Carlo, but due to uncertainties in event classification, a 60% systematic error is assigned to the Monte Carlo estimate. For the final cuts, the efficiency for muon identification and the hadron misidentification probability in $q\bar{q}$ events are shown in Table 2 in bins of p and $p_\perp$.

6 Measurement of the $b\bar{b}$ and $c\bar{c}$ Fractions

The measured lepton sample consists of contributions from seven sources: prompt leptons from decays of bottom hadrons, including $b \to lX$, $b \to \tau X \to lX'$, $b \to cX \to lX'$ ($l \equiv \{e, \mu\}$), prompt leptons from decays of charm hadrons, leptons from decays of light hadrons, electrons from photon conversions, and hadrons misidentified as electrons or muons. The high $p_\perp$ region, defined by the criteria $p_\perp > 2\,\mathrm{GeV/c}$ and $p > 3\,\mathrm{GeV/c}$, is dominated by b decays. Monte Carlo calculations predict that, in this region, 75% (71%) of the electrons

p	$p_\perp$	0-1	1-2	> 2
3-5	ϵ_μ	80±3	83±3	82±4
	ϵ_d	0.59±0.06	0.73±0.08	1.10±0.20
	ϵ_h	0.33±0.07	0.29±0.05	0.32±0.07
5-11	ϵ_μ	81±3	83±3	86±3
	ϵ_d	0.43±0.04	0.50±0.06	0.41±0.08
	ϵ_h	0.49±0.12	0.41±0.10	0.40±0.07
11-21	ϵ_μ	80±3	83±3	85±3
	ϵ_d	0.21±0.04	0.29±0.06	0.30±0.07
	ϵ_h	0.46±0.18	0.56±0.17	0.56±0.19

Table 2: Muon identification efficiency (ϵ_μ), the probability of contamination from $\pi^\pm$ or $K^\pm$ decay (ϵ_d) and the probability of hadron punch-through or sail-through (ϵ_h). All numbers are given in percent, while p and $p_\perp$ are in units of GeV/c.

(muons) are from b decay, 10% (9%) are from c decay, and 15% (20%) are from the non-prompt background and misidentification. In Section 7 this high-$p_\perp$ region is used, for electrons and muons, to extract $\Gamma_{b\bar{b}}$.

Almost 90% of the $c\bar{c}$ contribution is in the range $p_\perp < 2.0\,\mathrm{GeV/c}$. The $b\bar{b}$ contribution in this range is about 1.5 times that of $c\bar{c}$, but the two can be simultaneously measured, with a large negative correlation, by fitting over the full range of $p_\perp$. Since most of the background leptons also are in the low-$p_\perp$ range, extracting the $c\bar{c}$ contribution requires a good control of the background. By using electrons identified by both the ECAL and $\mathrm{d}E/\mathrm{d}x$, a very low misidentification background is achieved. Furthermore, the remaining misidentification background is accurately predicted by the method described in Section 4. Since the muon background at low $p_\perp$ is not as well understood, only electrons are used in the simultaneous fit to the $b\bar{b}$ and $c\bar{c}$ fractions, as described in Section 8.

To interpret the measured spectra, it is necessary to know the semileptonic branching ratios of the c and b quarks. The values used here are given in Table 3. The inclusive branching ratio for $c \to l\nu X$ is taken from an average of measurements made at PEP and PETRA, where the mix of D mesons and charm baryons is expected to be similar to that found at LEP. This branching ratio is necessary in order to compare the results for $c\bar{c}$ with the Standard-Model predictions, but since it is uncertain how best to do such an average over many experiments, the ALEPH measurement also is quoted

Branching Ratio		Reference
$b \to l\nu X$	0.102±0.007 (±0.007)	12
$b \to c \to l\nu X$	0.102±0.010 (±0.007)	13
$c \to l\nu X$	0.090±0.013	14
$b \to \tau\nu X$	0.05	15
$\tau \to l\bar{\nu}\nu$	0.175±0.004	16

Table 3: Values for branching ratios used in the fits of the inclusive lepton spectra (l refers to electrons or muons). The errors given in parentheses are our estimates of additional uncertainty due the different mixture of b hadrons at LEP as compared with that found in decays of the $\Upsilon(4S)$.

as $\mathrm{Br}(c \to e\nu X) \cdot \Gamma_{c\bar{c}}$. For the branching ratios $b \to l\nu X$ and $b \to c \to l\nu X$, the precise measurements made at the $\Upsilon(4S)$ are used [12,13]. Since these measurements were made from a sample with equal proportions of B_u and B_d mesons, the error estimates have been increased in order to account for uncertainty in the mixture of b hadrons produced at LEP energies. Nevertheless, since one cannot be sure to what extent the assumptions which were made are valid, the ALEPH measurements for $b\bar{b}$ are quoted as $\mathrm{Br}(b \to l\nu X) \cdot \Gamma_{b\bar{b}}$. The values assumed for the b semileptonic branching ratios are necessary only to make a comparison with the Standard-Model predictions and to extract the $c\bar{c}$ fraction.

7 Measurements from High-$p_\perp$ Leptons

In this section, results on the $b\bar{b}$ fraction and b fragmentation are obtained using only the high-$p_\perp$ region, in which muons and electrons may be used equally well. The best value for the $b\bar{b}$ fraction is taken to be a weighted average over the electron and muon results, while a comparison of the separate results yields an important cross check. In the high-$p_\perp$ analysis, electrons are not required to pass the $\mathrm{d}E/\mathrm{d}x$ cuts, because in this region of low background the reduction in background gained by $\mathrm{d}E/\mathrm{d}x$ would be compensated by a loss of efficiency, resulting in no net gain in the error on the final result.

To account for the small (10%) charm contribution, $\Gamma_{c\bar{c}}$ is constrained by the relation

$$2 \cdot \Gamma_{c\bar{c}} + 3 \cdot \Gamma_{b\bar{b}} = \Gamma_{\mathrm{had}}\,, \tag{8}$$

which follows from the assumption that the coupling is the same to all up-type quarks and, separately, to all down-type quarks. This assumption is more

conservative than using the value of $\Gamma_{c\bar{c}}$ as predicted by the Standard Model. Corrections to the coefficients in Eqn. 8 for kinematic effects and radiative corrections are not relevant when compared with the small size of the charm background and the present precision on the measurement of $\Gamma_{b\bar{b}}$.

Using the ECAL selection alone, from a sample of 24572 hadronic events, 328 high-$p_\perp$ electron candidates are identified. Likewise, from a sample of 20892 hadronic events, 237 high-$p_\perp$ muon candidates are identified in the barrel region of the detector. Their momentum distributions are shown in Figs. 4.a and 4.b, along with the predicted backgrounds from non-prompt leptons and misidentified hadrons, plus the Monte Carlo predictions for the $b\bar{b}$ and $c\bar{c}$ contributions. After background subtraction, 278 ± 19 electrons and 191 ± 17 muons remain from prompt b and c decays. The $b\bar{b}$ fraction times semileptonic branching ratio is measured to be, for electrons and muons respectively,

$$\begin{aligned} \mathrm{Br}(b \to e) \cdot \Gamma_{b\bar{b}}/\Gamma_{\mathrm{had}} &= 0.0217 \pm 0.0019(\mathrm{stat.}) \pm 0.0010(\mathrm{syst.}), \\ \mathrm{Br}(b \to \mu) \cdot \Gamma_{b\bar{b}}/\Gamma_{\mathrm{had}} &= 0.0238 \pm 0.0028(\mathrm{stat.}) \pm 0.0012(\mathrm{syst.}). \end{aligned} \quad (9)$$

The systematic errors are dominated by the uncertainties of 20% in the background normalization and 3% in the lepton identification efficiency.

As a cross check of the high-$p_\perp$ results, fits are made to the whole $p_\perp$ range, for electrons and muons, with the normalization of the predicted misidentification background allowed to float freely [19]. The $c\bar{c}$ fraction again is constrained according to Eqn. 8. The results show that the spectra at low $p_\perp$ are consistent with the high-$p_\perp$ regions which were used to extract the results for $\Gamma_{b\bar{b}}$. The background normalizations preferred by the fits are consistent with the Monte Carlo predictions for the muons and the measurements made using $\mathrm{d}E/\mathrm{d}x$ for the electrons.

The Monte Carlo simulation of the efficiency and background in the high-$p_\perp$ region depends on the assumptions used for b and c fragmentation. To account for this source of systematic error, ϵ_b and ϵ_c are fit from the observed lepton distributions. Taking electrons and muons together, a fit to the momentum distribution for $p_\perp > 2\,\mathrm{GeV/c}$ yields $\epsilon_b = 0.006^{+0.004}_{-0.003}$, and a fit to the p, $p_\perp$ distribution over the whole range of $p_\perp$ gives $\epsilon_c = 0.024^{+0.047}_{-0.022}$ [17]. The errors quoted here include systematic contributions. These results are consistent with previous measurements of charm and bottom fragmentation [10,18].

8 Combined Fit of the $b\bar{b}$ and $c\bar{c}$ Fractions

By using the TPC $\mathrm{d}E/\mathrm{d}x$ cuts in addition to the ECAL selection, the background at low $p_\perp$ can be reduced to a low enough level to allow a reliable fit of the $c\bar{c}$ fraction without the constraint of Eqn. 8. Some data runs for which

Fitted Variable	Value
$\Gamma_{c\bar{c}}/\Gamma_{\rm had}$	0.148 ± 0.044
$\Gamma_{b\bar{b}}/\Gamma_{\rm had}$	0.215 ± 0.017
$\langle x_c \rangle$	$0.52^{+0.11}_{-0.12}$
$\langle x_b \rangle$	$0.67^{+0.04}_{-0.03}$

Correlation Coefficients			
	$\Gamma_{c\bar{c}}/\Gamma_{\rm had}$	$\langle x_c \rangle$	$\langle x_b \rangle$
$\Gamma_{b\bar{b}}/\Gamma_{\rm had}$	-0.79	-0.46	0.09
$\Gamma_{c\bar{c}}/\Gamma_{\rm had}$		0.28	-0.04
$\langle x_c \rangle$			-0.58

Table 4: Results of the four-parameter fit to the electron p, $p_\perp$ spectrum. The errors given here are statistical only.

the dE/dx could not be properly calibrated were rejected, resulting in a sample of 22766 selected hadronic events, from which 1383 electron candidates are selected with $p > 2\,\mathrm{GeV/c}$.

A maximum likelihood fit, similar to that used in Ref. 20, is performed to the observed populations of the bins in p and $p_\perp$, with the signal above background accounted for by the four sources of prompt electrons. Four parameters, the fractions of $b\bar{b}$ and $c\bar{c}$ events and the average x of b and c hadrons, $\langle x_b \rangle$ and $\langle x_c \rangle$, are allowed to vary independently, where x is defined to be the ratio of the hadron energy to the LEP beam energy. For each of the four sources of prompt electrons and for each of six bins in x of the c and b hadrons, Monte Carlo simulation is used to predict the probability of detecting a prompt electron in each of the p, $p_\perp$ bins. The shapes of the x distributions of the c and b hadrons are assumed to follow the form given in Eqn. 1, with z replaced by x. The results of the fit are not sensitive, at the present level of statistical precision, to the detailed form used to describe the x distribution. For example, if the form $f(x) = x^\alpha(1-x)$, with α a free parameter, is instead used, the fit results change by less than one half of a standard deviation in the statistical error.

The detailed results of the fit, for $p > 2\,\mathrm{GeV/c}$, are summarized in Table 4. In Fig. 5.a and 5.b are plots of the measured p, $p_\perp$ spectrum projected on the p and $p_\perp$ axes. Also shown are the results of the fit, separated into the two components of the background plus the primary $c\bar{c}$ contribution and the $b\bar{b}$ contribution. A χ^2 test on the 30 bins in p, $p_\perp$ used in the fit gives a confidence level of 41%.

Systematic errors are determined by allowing branching ratios, background, and efficiency to vary within their allowed ranges. Both the normalization of the misidentification background and its slope in momentum are allowed to vary within the limits imposed by the measurements of Table 1, resulting in a 2% error on $\Gamma_{b\bar{b}}$ and a +12%, −6% error on $\Gamma_{c\bar{c}}$. The prediction of the

background from non-prompt electrons results in a 7% error on $\Gamma_{c\bar{c}}$, but only a 1% error on $\Gamma_{b\bar{b}}$. The uncertainty in the branching ratio for $b \to e\nu X$ gives a 14% error on $\Gamma_{c\bar{c}}$, while the uncertainty in the branching ratio for $c \to e\nu X$ gives a negligible contribution to the error on $\Gamma_{b\bar{b}}$. Likewise, the uncertainty in the branching ratio for $b \to c \to e\nu X$ gives an error of $+19\%$, -16% on $\Gamma_{c\bar{c}}$ but no significant error on $\Gamma_{b\bar{b}}$. A 4% error on both partial widths arises from the uncertainty in the efficiency for detection and identification of electrons. Adding all systematic errors in quadrature gives

$$\begin{aligned} \mathrm{Br}(b \to e) \cdot \Gamma_{b\bar{b}}/\Gamma_{\mathrm{had}} &= 0.0219 \pm 0.0017(\mathrm{stat.}) \pm 0.0010(\mathrm{syst.}), \\ \mathrm{Br}(c \to e) \cdot \Gamma_{c\bar{c}}/\Gamma_{\mathrm{had}} &= 0.0133 \pm 0.0040(\mathrm{stat.})^{+0.0038}_{-0.0031}(\mathrm{syst.}), \\ \langle x_b \rangle &= 0.67^{+0.04}_{-0.03}, \\ \langle x_c \rangle &= 0.52^{+0.16}_{-0.15}. \end{aligned} \tag{10}$$

The errors quoted for $\langle x_c \rangle$ and $\langle x_b \rangle$ include the systematic contributions. Also, note that the "statistical" errors on $\Gamma_{b\bar{b}}$ and $\Gamma_{c\bar{c}}$ include the contributions from fragmentation, since $\langle x_c \rangle$ and $\langle x_b \rangle$ are allowed to vary freely in the fit.

This result for the $b\bar{b}$ fraction is in good agreement with the analyses of the previous section, in which only the high-$p_\perp$ region is used and the $c\bar{c}$ contribution is constrained according to Eqn. 8. The fitted values of $\langle x_b \rangle$ and $\langle x_c \rangle$ also are consistent with the values for ϵ_b and ϵ_c obtained in the previous section (which correspond to $\langle x_b \rangle = 0.68$ and $\langle x_c \rangle = 0.51$ respectively, when used with the JETSET parton shower model).

9 Conclusion

From inclusive electron and muon production, the $b\bar{b}$ and $c\bar{c}$ fractions in hadronic Z decays have been measured. The results obtained for the $b\bar{b}$ fraction from high-$p_\perp$ electrons and muons are presented separately in Eqn. 9. Taking a weighted average of the two gives

$$\mathrm{Br}(b \to e) \cdot \Gamma_{b\bar{b}}/\Gamma_{\mathrm{had}} = 0.0224 \pm 0.0016(\mathrm{stat.}) \pm 0.0010(\mathrm{syst.}). \tag{11}$$

To quote a result for $\Gamma_{b\bar{b}}/\Gamma_{\mathrm{had}}$, the b semileptonic branching ratio from Table 3 is assumed, giving

$$\Gamma_{b\bar{b}}/\Gamma_{\mathrm{had}} = 0.220 \pm 0.016(\mathrm{stat.}) \pm 0.024(\mathrm{syst.}), \tag{12}$$

where the systematic error is dominated by the uncertainty in the semileptonic branching ratio. This result is in good agreement with the Standard-Model prediction of $\Gamma_{b\bar{b}}/\Gamma_{\mathrm{had}} = 0.217$ [21] (for $M_Z = 91.18\,\mathrm{GeV/c^2}$ [1], $\alpha_s = 0.12$, $M_{\mathrm{top}} = 150\,\mathrm{GeV/c^2}$, and $M_{\mathrm{Higgs}} = 100\,\mathrm{GeV/c^2}$).

Moreover, due to the purity of the sample of electrons obtained by using both the ECAL and dE/dx, along with the precise estimate from data of the remaining hadron background, ALEPH is able to make the first measurement of the $c\bar{c}$ fraction in hadronic Z decays. Since the $c\bar{c}$ and $b\bar{b}$ contributions to the electron spectrum are fit simultaneously, the $b\bar{b}$ fraction also is obtained without making any assumptions about the Z coupling to $c\bar{c}$. The results for the $b\bar{b}$ and $c\bar{c}$ fractions times semileptonic branching ratios are given in Eqn. 10. Using the branching ratios from Table 3 yields

$$\begin{aligned} \Gamma_{b\bar{b}}/\Gamma_{\rm had} &= 0.215 \pm 0.017(\text{stat.}) \pm 0.024(\text{syst.}), \\ \Gamma_{c\bar{c}}/\Gamma_{\rm had} &= 0.148 \pm 0.044(\text{stat.})^{+0.045}_{-0.038}(\text{syst.}). \end{aligned} \tag{13}$$

The $b\bar{b}$ fraction is in excellent agreement with the high-$p_\perp$ measurement, in which $\Gamma_{c\bar{c}}$ is constrained according to Eqn 8. The $c\bar{c}$ fraction agrees with the Standard-Model prediction of $\Gamma_{c\bar{c}}/\Gamma_{\rm had} = 0.171$ [21].

10 Acknowledgements

We would like to thank our colleagues of the LEP division for the outstanding performance of the LEP accelerator. Thanks are also due to the many engineering and technical personnel at CERN and at the home institutes for their contributions towards ALEPH's success. Those of us not from member states wish to thank CERN for its hospitality.

References

[1] D. Decamp *et al.*, ALEPH Collab., Phys. Lett. B **231** (1989) 519; Phys. Lett. B **235** (1990) 399.

[2] B. Adeva *et al.*, L3 Collab., Phys. Lett. B **231** (1989) 509;
P. Aarnio *et al.*, DELPHI Collab., Phys. Lett. B **231** (1989) 539;
M.Z. Akrawy *et al.*, OPAL Collab., Phys. Lett. B **231** (1989) 530.

[3] S.L. Glashow, Nucl. Phys. **A22** (1961) 579;
S. Weinberg, Phys. Rev. Lett. **19** (1967) 1264;
A. Salam, *Elementary Particle Theory*, ed. N. Svartholm, Stockholm, Almquist and Wiksell (1968), 367.

[4] J.F. Kral *et al.*, Mark II Collab., Phys. Rev. Lett. **64** (1990) 1211.

[5] B. Adeva *et al.*, L3 Collab., L3 Preprint 6 (1990).

[6] D. Decamp *et al.*, ALEPH Collab., CERN-EP/90-25, submitted to Nucl. Inst. Meth.

[7] J.E. Campagne, Ph.D. Thesis, Paris, LPNHEP 89-02;
J.E. Campagne and R. Zitoun, Z. Phys. C, **43** (1989) 469.

[8] T. Sjöstrand and M. Bengtsson, Comp. Phys. Com. **43**, 367 (1987).

[9] C. Peterson *et al.*, Phys. Rev. **D27** (1983) 105.

[10] J. Chrin, Z. Phys. C **36** (1987) 163;
W. Bartel *et al.*, Z. Phys. C **33** (1987) 339.

[11] W. Bartel *et al.*, Z. Phys. C, **33** (1986) 23, S. Bethke *et al.*, Phys. Lett. **B213** (1988) 235. We use a value of $y_{\rm cut} = 0.02$ for the clustering algorithm.

[12] For the b semileptonic branching ratio, we use an average of the CLEO and ARGUS results presented by K.R. Schubert in *Review of B-Meson Decay Results*, **1989 Int. Symp. on Heavy Quark Physics**, ed. by P.S. Drell and D.L. Rubin, AIP Conf. Proc. 196, Am. Inst. of Phys., New York (1989) p. 79. Since the spectator model generally gives a good description of observed B meson decays (for example, the measured result $\tau(B^+)/\tau(B^0) = 1.0 \pm 0.2$), we assume that the average semileptonic rate at LEP energies is the same as that observed at the $\Upsilon(4S)$. However, since the mixture of b hadrons from the Z differs from that from the $\Upsilon(4S)$, any variation in lifetime among the b hadrons will result in a systematic error in the average semileptonic rate. We account for this by introducing an additional systematic error of 7%, assuming a rate of 10% for b-baryon production and relative B-meson production rates of $B^+ : B^0 : B_s :: 1 : 1 : 0.3$. The b-baryon lifetimes are assumed to be within a factor of 2 of the B-meson lifetime.

[13] For the branching ratio $b \to c \to l\nu X$, we use the CLEO result (J. Alexander in *Les Rencontres de Physique de la Vallée d'Aosta, La Thuile*, March 1990. This result is to be published in Phys. Rev. D), obtained from their fit to the lepton spectrum from the $\Upsilon(4S)$. We introduce an additional systematic error of 7% by considering the expected differences in the B-meson mixture between Z decays and $\Upsilon(4S)$ decays, as mentioned in [12].

[14] For the c semileptonic branching ratio, we calculate an average of the electron and muon results from the following references:
B. Adeva *et al.*, MARK J Collab., Phys. Rev. Lett. **51** (1983) 443;
H.J. Berend *et al.*, CELLO Collab., Z. Phys. C **19** (1983) 291.
E. Fernandez *et al.*, MAC Collab., Phys. Rev. Lett. **50** (1983) 2054;

M. Althoff *et al.*, TASSO Collab., Z. Phys. C **22** (1984) 219; Phys. Lett. **146B** (1984) 443;
H. Aihara *et al.*, TPC Collab., Phys. Rev. **D31** (1985) 2719; Z. Phys. C **27** (1985) 39;
T. Pal *et al.*, DELCO Collab., Phys. Rev. **D33** (1986) 2708;
W. Bartel *et al.*, JADE Collab., Z. Phys. C **33** (1987) 339;
R. Ong *et al.*, Mark II Collab., Phys. Rev. Lett. **60** (1988) 2587.

[15] C. Quigg and J.L. Rosner, Phys. Rev. **D19** (1979) 1532.

[16] G.P. Yost *et al.*, Phys. Lett. **B204** (1988) 13.

[17] The values we have used for the parameters Λ and $M_{\text{min.}}$ of the Lund JETSET 6.3 parton-shower model are $\Lambda = 0.35\,\text{GeV}$ and $M_{\text{min.}} = 1.46\,\text{GeV/c}^2$.

[18] S. Bethke, Z. Phys. C, **29** (1985) 175; HD-PY 86/07 (1986).

[19] P. Perret, Ph.D. Thesis, Université Blaise Pascal, Clermont-Ferrand, France (1990).

[20] M. Nelson, *Inclusive Lepton Production in Hadronic Events from e^+e^- Annihilation at 29 GeV*, Ph.D. Thesis, University of California, Berkeley, LBL-16724 (1983).

[21] F.A. Berends *et al.*, Nucl. Phys. **B297** (1988) 429;
W. Beenakker and W. Hollik, in **ECFA workshop on LEP 200**, CERN Report 87-08 (1987) p. 185, ed. by A. Boehm and W. Hoogland;
W. Hollik, DESY 88-188 (1988).

Figure Captions

Figure 1 Variables for electron identification in hadronic events. a.) ECAL: the momentum-energy balance variable R_T as a function of momentum, after cutting on the longitudinal profile variable R_L. b.) TPC: the number of standard deviations, R_I, from the dE/dx electron hypothesis as a function of momentum, after selecting electron candidates according to the ECAL selection variables R_T and R_L.

Figure 2 a.) A comparison between Monte Carlo and data for the distribution of the momentum-energy balance variable R_T for all tracks with $p > 2\,\mathrm{GeV/c}$, after cutting on the longitudinal profile variable R_L. The discrepancy between Monte Carlo and data is discussed in Section 4. b.) The distribution of R_I for all tracks, with $3 < p < 7\,\mathrm{GeV/c}$, passing the ECAL electron selection of Eqn. 6. The data are fit to a Gaussian curve, to describe the signal, plus a background shape derived from the R_I distribution of all tracks failing the ECAL electron selection.

Figure 3 Comparison between data and Monte Carlo of the number of fired planes in the last 10 planes of the HCAL, for those tracks satisfying all the muon identification cuts except the requirements on the number of hits in the last 10 planes.

Figure 4 Momentum spectrum of leptons with $p_\perp > 2\,\mathrm{GeV/c}$: a.) electrons selected by ECAL, b.) muons. Along with the data are plotted the Monte Carlo predictions for the signal and background, corresponding to the measured value of $\Gamma_{b\bar{b}}/\Gamma_{\mathrm{had}}$.

Figure 5 Comparison of fit and data for electrons selected by ECAL plus dE/dx: a.) momentum distribution, b.) transverse momentum distribution for $p > 2\,\mathrm{GeV/c}$. The definition of transverse momentum is given in Section 3.

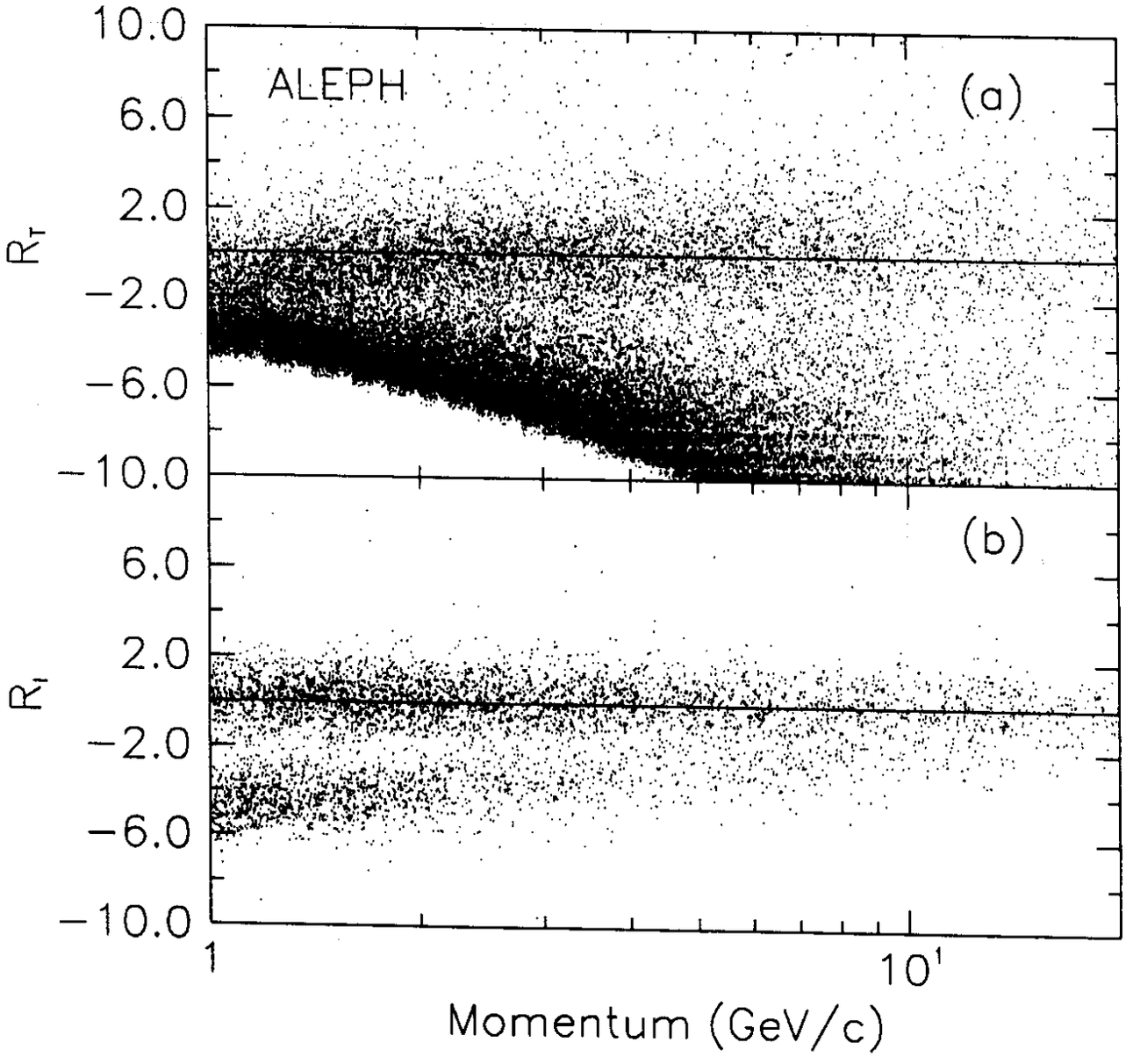

Fig. 1

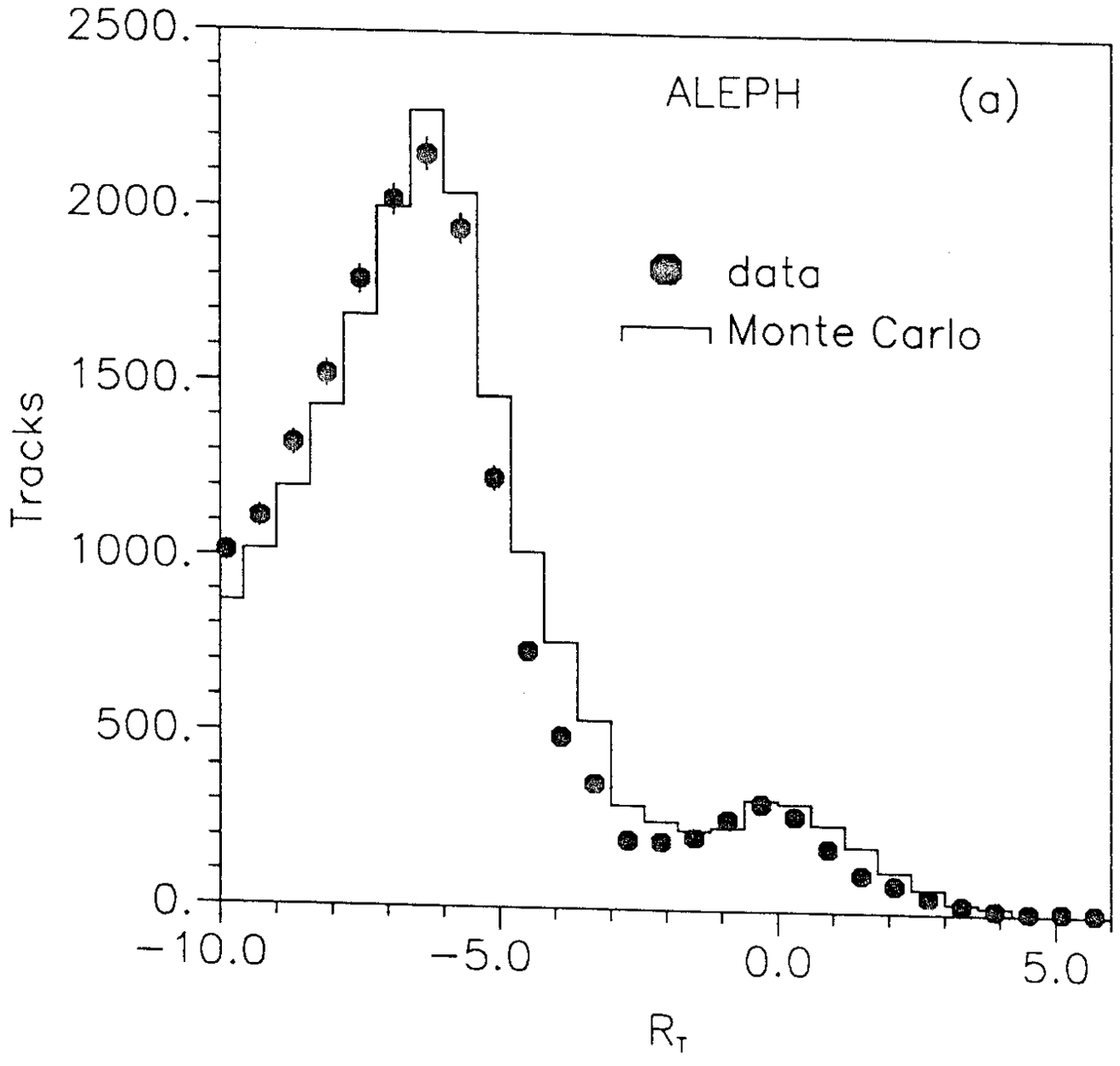
ALEPH
(a)
data
Monte Carlo
Tracks
2500.
2000.
1500.
1000.
500.
0.
−10.0
−5.0
0.0
5.0
R_T

Fig. 2.a

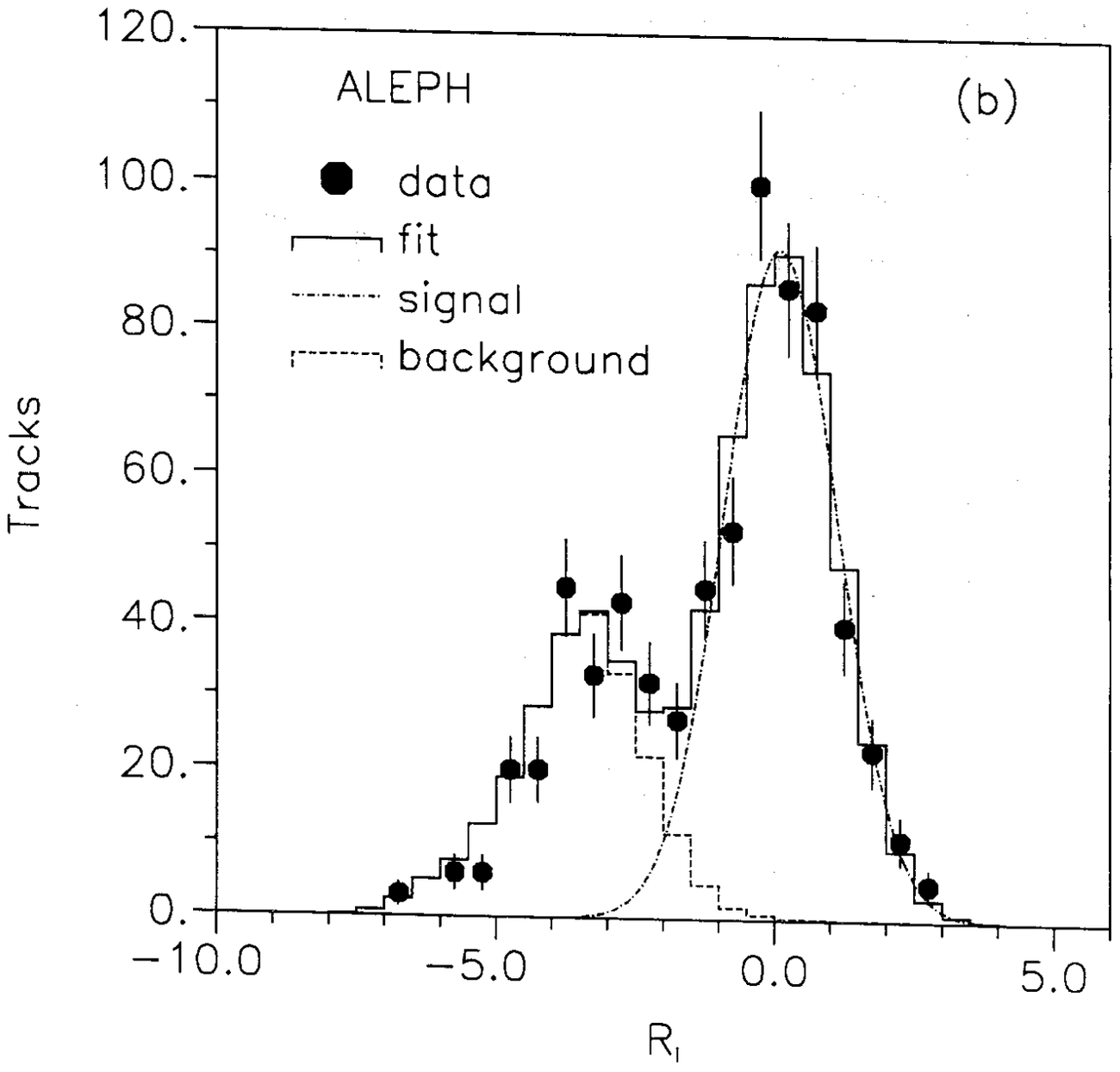
ALEPH
(b)
data
fit
signal
background
Tracks
120.
100.
80.
60.
40.
20.
0.
−10.0
−5.0
0.0
5.0
R_l

Fig. 2.b

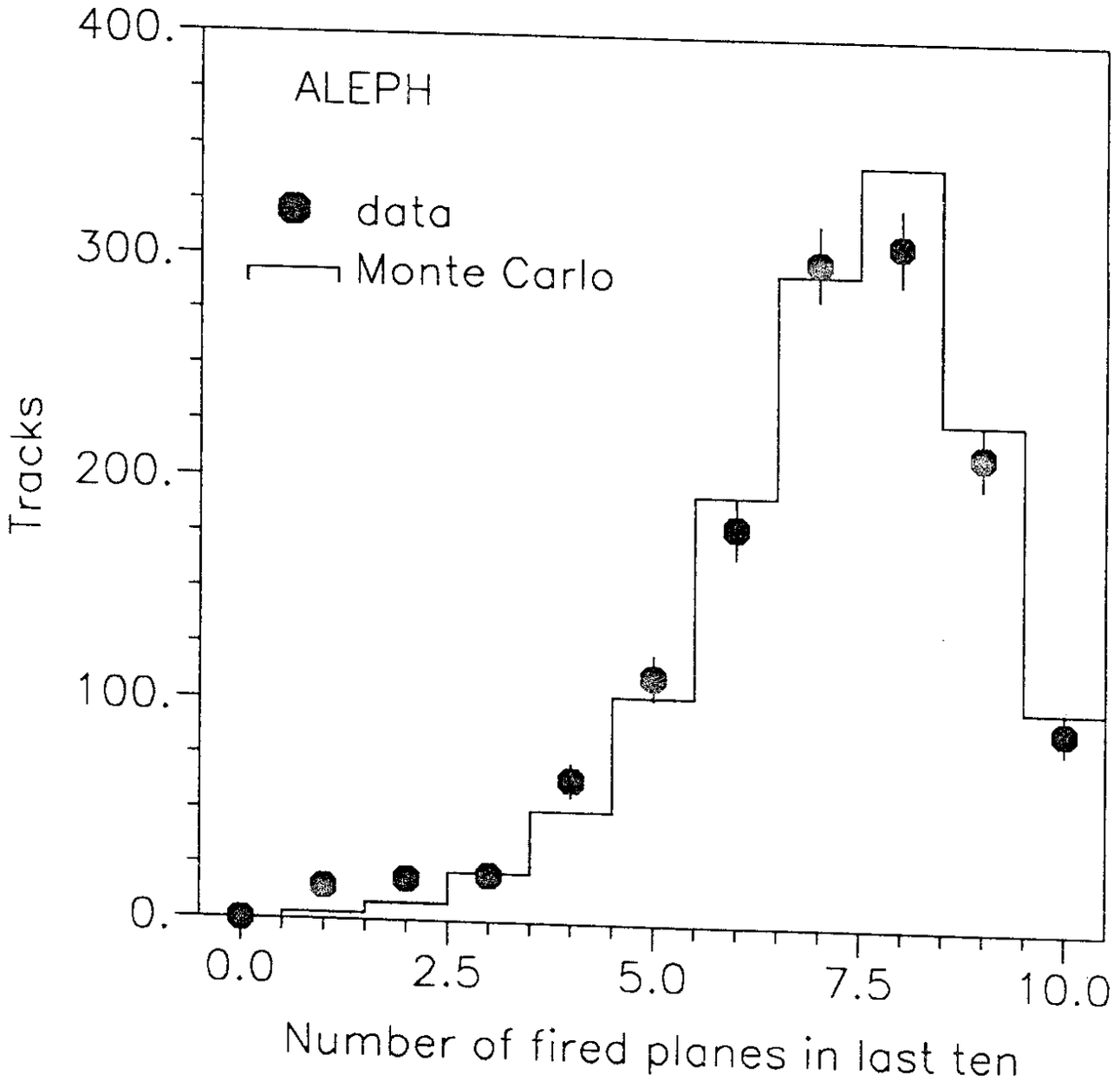
400.
300.
200.
100.
0.
Tracks
ALEPH
data
Monte Carlo
0.0
2.5
5.0
7.5
10.0
Number of fired planes in last ten

Fig. 3

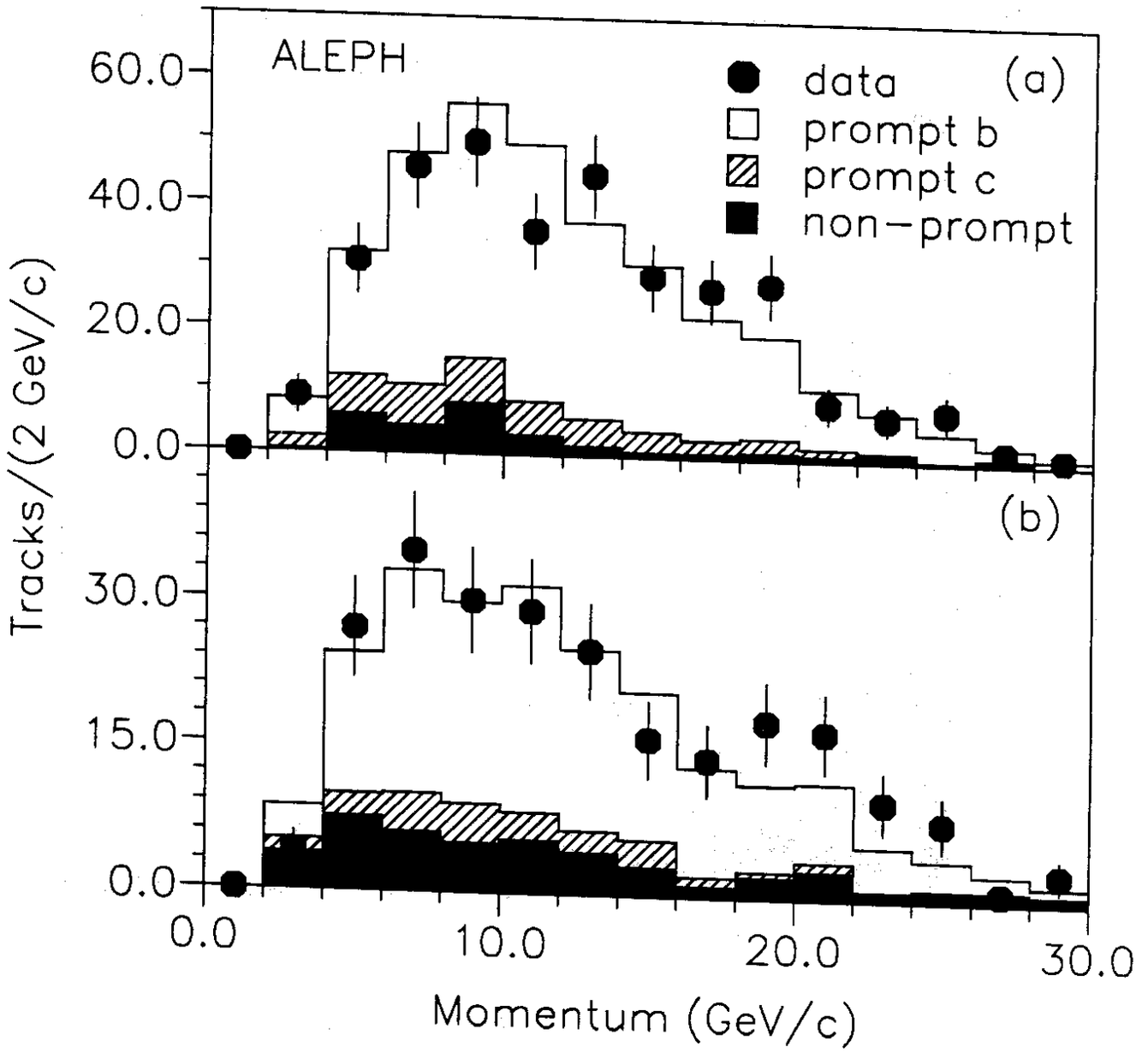
ALEPH
data
prompt b
prompt c
non−prompt
(a)
(b)
60.0
40.0
20.0
0.0
30.0
15.0
0.0
0.0
10.0
20.0
30.0
Tracks/(2 GeV/c)
Momentum (GeV/c)

Fig. 4

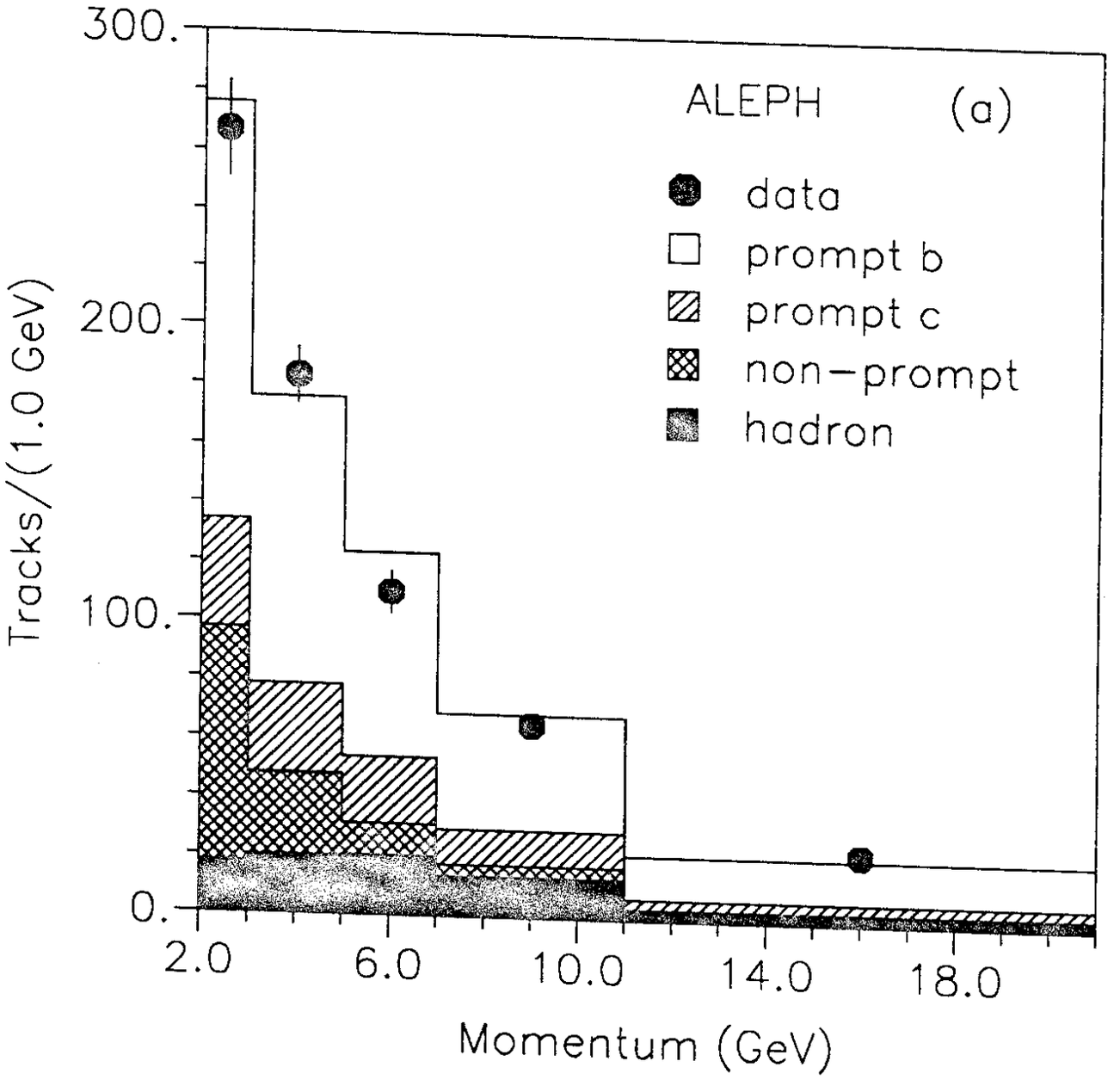
ALEPH
(a)
data
prompt b
prompt c
non−prompt
hadron
Tracks/(1.0 GeV)
300.
200.
100.
0.
2.0
6.0
10.0
14.0
18.0
Momentum (GeV)

Fig. 5.a

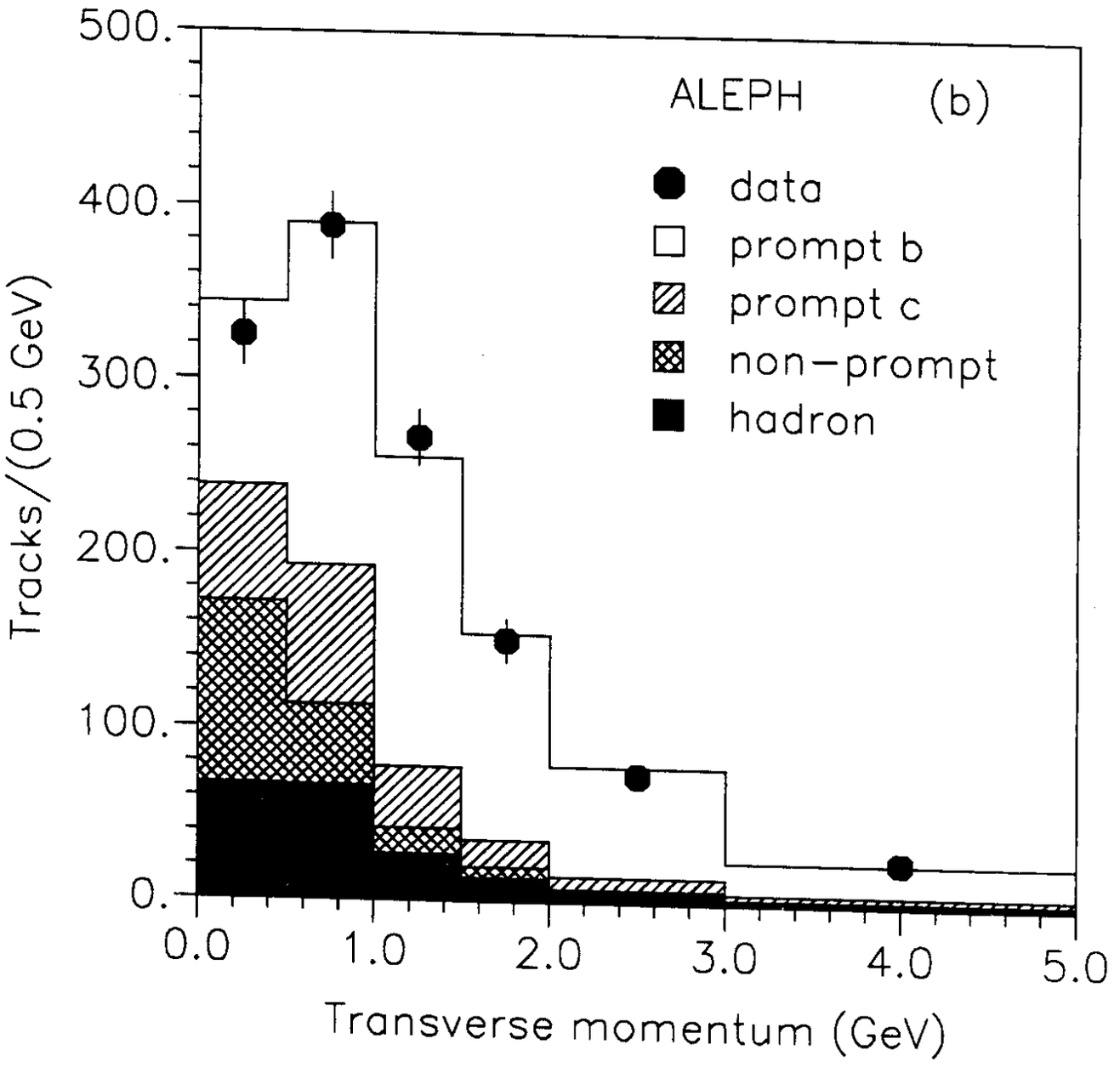
ALEPH (b)
data
prompt b
prompt c
non−prompt
hadron
Tracks/(0.5 GeV)
500.
400.
300.
200.
100.
0.
0.0
1.0
2.0
3.0
4.0
5.0
Transverse momentum (GeV)

Fig. 5.b